Micro- and Nanofibrillated Cellulose as a Rheology Modifier Additive in CMC-Containing Pigment-Coating Formulations

ARTICLE *in* INDUSTRIAL & ENGINEERING CHEMISTRY RESEARCH · OCTOBER 2013

Impact Factor: 2.59 · DOI: 10.1021/ie4028878

3 AUTHORS, INCLUDING:

Katarina Dimic-Misic
Aalto University
22 PUBLICATIONS **83** CITATIONS
SEE PROFILE

Jouni Paltakari
Aalto University
42 PUBLICATIONS **331** CITATIONS
SEE PROFILE

I&EC research
Industrial & Engineering Chemistry Research

Article

pubs.acs.org/IECR

Micro- and Nanofibrillated Cellulose as a Rheology Modifier Additive in CMC-Containing Pigment-Coating Formulations

K. Dimic-Misic,*[,†] P. A. C. Gane,[†,‡] and J. Paltakari[†]

[†]School of Chemical Technology, Department of Forest Products Technology, Aalto University, P.O. Box 16300, FI-00076 Aalto, Finland

[‡]Omya International AG, Baslerstrasse 42, CH-4665 Oftringen, Switzerland

ABSTRACT: Suspension rheology of aqueous coatings influences the coating application performance at high speeds and during high rates of change of the shear rate, as well as the quality of the coated end product determined by the relationship between dewatering, immobilization, and coating coverage. In the case of paper coatings, the end-use printing can be significantly affected by the coating uniformity, pore structure, and surface chemistry. Nanocellulose-containing materials, such as microfibrillated (MFC) and nanofibrillated (NFC) cellulose, are potential additives that could at least partly substitute other natural and synthetic cobinders, including viscoelasticity-inducing starch, carboxymethyl cellulose (CMC), and polyacrylic thickeners, in paper-coating color formulations. Work is reported here in which a systematic comparison of dewatering and rheological characteristics of coating colors, based on three different pigments and mixtures thereof, is illustrated using CMC as the cobinder and incorporated with MFC/NFC as the partial cobinder replacement. All colors are shown to exhibit viscoelasticity, but the MFC/NFC additives are seen to operate as water-binding gel-forming components rather than with the flocculating thickening action of CMC. Immobilization of the color in the presence of nanofibrillar material is identified as the point of gel−water entrapment rather than the traditional stick−slip particle−particle interlocking mechanism predominating in traditional flocculant thickener formulations.

INTRODUCTION

Cellulose is widely used in the form of microfibers, but recently there has been significant interest in both academia and the industry concerning the production of cellulosic materials having components with characteristic size on the nanometer scale. These are being considered as a major potential contribution to the economic future of the forest products industry.[1] Microfibrillated (MFC) and nanofibrillated (NFC) cellulose are examples of such nanocellulose-containing materials, present in lesser or greater amounts, respectively, and they possess distinctly different properties compared to standard macroscopic fibers. Such properties, including very high mechanical strength and elastic modulus, low thermal expansion, among others, are due primarily to their self- and water-interactive properties, in turn related to the high surface area and unique optical and self-assembly characteristics.[2,3] The geometric properties of the intrinsic nanocellulose structures (shape, length, and diameter) depend mainly on the extraction process and on the origin of the cellulose raw material.[4−6] Cellulose micro/nanofibers can be obtained from mechanical and/or chemical procedures. Among the mechanical procedures, the following can be mentioned to exemplify: refining or high-shear homogenizing,[7,8] microfluidizing,[9] and sonication,[3] which result in mechanically ground and/or separated micro- and nanofibrils. Refinement and homogenization are carried out in the presence of water, usually producing micro/nanofibrils by passing the suspension of pulp fibers through a relatively narrow gap of a disk apparatus between the rotor and stator. In the microfluidising process, the suspension is subject to high pressure to force passage through a Y- or Z-type geometry flow chamber.[9] Sonication is carried out in a fiber suspension in order to separate the micro/nanofibril bundles in the fiber cell wall through cavitation.[10] Among the chemical procedures, the following can be highlighted: enzymatic hydrolysis with cellulases,[11] leading to micro- and nanofibrils, and selective oxidation of primary hydroxyl groups into carboxylate groups, leading to the production of high-aspect-ratio fibrils (TEMPO).[12] This resulting high aspect ratio describes fibrils possessing a diameter varying between 5 and 100 nm, depending on the details of the production process and raw materials. The typical size of NFC is smaller and its surface charge much higher compared to those of MFC. Nanocrystalline cellulose, as opposed to micro/nanofibrillar cellulose, is produced by acid hydrolysis to form an essentially fibril-free material.[13]

Nanofibrillar and nanocrystalline cellulose bind water strongly, and retained fiber structures in the fibrillar case swell in the presence of water. The result is a gel-like structure, which acts partially as a voluminous medium in the suspension.[14,15]

Nanocellulosic materials, such as those from the production routes described above, are expected to influence traditional coating layer properties, especially those designed for specific purposes, such as absorbency and/or permeability as well as forming selective barriers to liquids. The observation that nanocellulose could be used in paper-coating formulations, as a cobinder for example, based on its biodegradable nature as well

Received: September 3, 2013
Revised: October 14, 2013
Accepted: October 15, 2013
Published: October 15, 2013

as strong shear-thinning properties, raises a question about the possible processability of MFC/NFC-containing coatings. In a high-speed coating process (>1000 m·min^{-1}), dependency primarily on high rates of change of the shear rate results in manifestation of the viscoelasticity and sensitivity to pressure-pulse dewatering when applied to a permeable substrate. In slower-speed applications, the capillary-driven dewatering on absorbent substrates dominates, and the nature of the progress toward coating immobilization on the surface is the critical factor.[16−18] Controlling precisely the increase in the solids content of coating colors, particularly under pressure-pulse conditions, is an important aspect for running high solids coatings designed at reducing the production cost, as well as impacting such properties as coating layer coverage and optical characteristics. The mechanism of faster immobilization, resulting in lower demand and reduced reswelling of fibers in the base paper surface, is a regular target for improved coating performance including savings in drying energy.[18−20] Coating color formulations have been continuously optimized in order to maximize the solids content, which, if not accompanied by the correct control of rheology and dewatering, frequently results in a negative impact on the coating processability through excessive blade load, blade bleeding, and stalagmite formation, streaking, and scratches, among other things, leading to higher numbers of web breaks and unacceptable coating layer irregularities.[21,22] The high rate of change of the strain rate under shear conditions is affected by the coater speed and wet film thickness, which are, themselves, affected by the coating color elasticity and water retention properties.

At the highest coating speeds or highest coating color solids content, the short-time-scale response of the viscoelastic color under the rapid rates of change of induced stress becomes critical.[16,23,24] The viscoelasticity, arising from the colloidal and structural interactions of the coating color components, results in the coating color behaving more as an elastic solid than a viscous liquid, which then imposes a plug-flow regime supported by boundary slip under the coating blade nip.[16] Boundary slip is also supported by the formation of boundary water layers: a characteristic of gel-like materials when sheared under fixed geometry and something that is suspected to be typical of nanocellulosic waterborne materials such as those studied in this work.[25] Loss of water under the pressure pulse of the blade exacerbates the viscoelastic property in the region before the high rate of change of induced stress at the blade.[16,25] Rapid removal of water, however, can induce some desirable immobilization of the coating color at the base−paper interface, but too fast pressure-pulse dewatering can lead to undesirable effects such as binder migration, i.e., nonuniform binder distribution within and along the coating layer.[17,22,26] Besides elasticity, the shear-thinning properties of a coating color describe its behavior under pumping and distribution to the coating machine head.

In this study, MFC and NFC are used to substitute, at least partially, the standard cobinder material carboxymethyl cellulose (CMC). We focus on how MFC/NFC, utilized as a cobinder in the coating formulation, influences its rheological behavior, bearing in mind that such nanocellulosic materials act to form gels in water as opposed to inducing the flocculation behavior of color components known to occur with CMC.[16,27−32]

MATERIALS

To help characterize the constituents of the coatings, the charge of the pigments was determined by a Zeta-sizer (Malvern Instruments Ltd.). The average particle size of the pigments MFC and NFC was measured with dynamic light scattering (DLS), using the photon correlation spectroscopic technique with a Zeta-sizer (Malvern Instruments Ltd.). Prior to measuring the ζ potential (Ψ_z) and ensemble average particle size, the samples were diluted with deionized water to a solid content of 0.01%.

Pigments used in this work were in predispersed slurry form. Two ground calcium carbonates (GCCs), produced by wet grinding in the presence of polyacrylate dispersant, and a high-aspect-ratio sedimentary clay were studied. The two GCCs were respectively a relatively coarse Hydrocarb 60 (cGCC) and a finer Hydrocarb 90 (fGCC) (Omya AG, Switzerland). The cGCC grade had 60% w/w of particles <2 μm, with a weight median diameter of 1.35 μm and ζ potential Ψ_z of −27.13 mV at pH 9.2. The finer fGCC had 90% w/w of particles <2 μm with a weight median diameter of 0.7 μm having a Ψ_z value of −25.4 mV at pH 8.9. The high-aspect-ratio Brazilian rotogravure kaolin clay, Capim RG (supplied by Imerys, St. Austell, Cornwall, U.K.) in slurry form (66% w/w solids content), had an ISO brightness of 88.5, with 55% w/w of particles <2 μm, a shape factor aspect ratio (platiness) of ∼40, and a Ψ_z value of −45.33 mV at pH 8.5.

Three different thickener/cobinder systems were used in this work: a carboxymethyl cellulose (CMC; Finnfix 10, Kelco, Finland), which in the further test coating colors is partially replaced by microfibrillated (MFC) and nanofibrillated (NFC) cellulose, respectively. CMC had a molecular weight of 66 kg·mol^{-1} and a degree of substitution of 0.78. A styrene acrylic latex (SA-Latex), Styron XZ 96 767.00, was used as the binder, having a glass transition temperature T_g of 24 °C, a minimum film-forming temperature (MFFT) of 20 °C, a particle size of 105 nm, a dry solids content of 50% w/w, pH 8.0, and a viscosity of 320 mPa·s (Styron Suomi Oy, Hamina, Finland), as reported by the supplier.

MFC was prepared by grinding Birch Kraft pulp with an ultrafine friction grinder (Masuko Supermasscolloider, MKZA 10-15J) equipped with SiC grinding stones (MKE10-46). Light transmittance for 0.1% consistency at a wavelength of 800 nm was 34.3%. The average particle size of the agglomerates was 6692 nm as measured by DLS. The sample NFC was produced in a pilot process by oxidation and then fibrillation. A TEMPO catalyst was used in oxidation of the Birch Kraft pulp.[12] The average size of the agglomerates, measured with DLS, was 977 nm. The carboxylic acid content on NFC was 0.1 mmol·g^{-1} as determined by conductometric titration.[33] NFC had a degree of substitution of 0.2 and was delivered at 2.3% consistency.

Any retained fiber portion in MFC/MFC swells when in contact with water. The nanofibrillar material combines with water to form a gel, containing water within its interparticle nanoporous structure. The difference in the water−binding property, relating to the nanoporous structure of MFC and NFC, was evaluated with a water retention value test (WRV ISO/DIS 23714), which was modified with respect to sample preparation to suit the measurement of nanocellulose.[34] This was done by mixing quantities of nanocellulose in the range 0−6% with an unrefined Kraft pulp and then centrifuging the mixture under normal WRV test conditions. The curve of WRV against the nanocellulose content was used to extrapolate to the

dx.doi.org/10.1021/ie4028878 | Ind. Eng. Chem. Res. 2013, 52, 16066−16083

Table 1. Coating Color Formulations[a]

	cGCC/ ref	cGCC/ MFC	cGCC/ NFC	fGCC/ ref	fGCC/ MFC	fGCC/ NFC	75 cGCC/ ref	75 cGCC/ MFC	75 cGCC/ ref	50 cGCC/ CMC	50 cGCC/ ref	50 cGCC/ NFC	100 clay/ ref	100 clay/ MFC	100 clay/ NFC
cGCC	100	100	100	0	0	0	75	75	75	50	50	50	100	100	100
fGCC	0	0	0	100	100	100	0	0	0	0	0	0	0	0	0
clay	0	0	0	0	0	0	25	25	25	50	50	50	100	100	100
SA-latex	15	15	15	15	15	15	15	15	15	15	15	15	15	15	15
CMC	0.4	0.1	0.1	0.4	0.1	0.1	0.4	0.1	0.1	0.4	0.1	0.1	0.4	0.1	0.1
MFC	0	0.3	0	0	0.3	0	0	0.3	0	0	0.3	0	0	0.3	0
NFC	0	0	0.3	0	0	0.3	0	0	0.3	0	0	0.3	0	0	0.3

[a]Component amounts are given in parts per hundred (pph; by weight) based on 100 parts by weight of pigment(s). Complementary to the GCC portion is the kaolin (clay) in all clay-containing formulations in order to form 100 pph pigment.

pure nanocellulose swelling. The water retained in NFC and MFC at a 2% content was found to be 24 and 9 g of water/g of solids, respectively. The surface charge and fine structure of NFC largely explain its higher water binding property, effectively exerting a stronger surface wetting and capillary action than the centrifugal force used for dewatering in the WRV test.

Suspensions of cellulose fibers and nanocellulose were prepared for individual analysis at four different concentrations (1.0%, 1.5%, 2.0%, and 2.3%, respectively). Different consistencies of MFC and NFC suspensions were obtained by dilution of the initial stock concentrations of 3.0% and 2.3%, respectively. Dilutions were made using deionized water. The suspensions were labeled according to their consistency and type with respect to the material content (MFC/NFC). The final pH of all suspensions was between 8.0 and 8.2.

Preparation and Characterization of the Coating Colors. The relative amount of each ingredient in the coating color formulations is shown in Table 1. The dry solid content was 63% w/w for all coating colors. CMC was prepared as an aqueous solution of 10% w/w. The coating colors were prepared by mixing of the pigment slurries with SA-Latex under agitation in a Diaf mixer (Pilvad Diaf A/S, Humlebæk, Denmark) at 900 min^{-1} for 15 min, and then the cobinder was added (CMC and MFC/NFC) using the same rotation speed for 25 min. The coating color pH values were in the range 8.5−9.0.

METHODS

Rheometry. The viscoelastic rheological investigations were performed at 23 °C by means of an Anton Paar 300 (Anton Paar Germany GmbH, Ostfildern-Scharnhausen, Germany) oscillatory constant stress/strain and variable shear rheometer.[35,36] The parallel-plate geometry was selected with an upper plate diameter of 50 mm, with the gap between the upper and bottom plates being 1 mm. Prior to measurement, the sample was presheared at an angular frequency of 10 rad·s^{-1} and a strain deformation of 0.1% for 10 min, followed by a rest stationary state time of 15 min.[37,38] Different types of rheological measurements were performed on the same rheometer, preserving the geometry, viscoelastic measurements, stability and recovery tests,[35,36,39] and steady-state flow with increasing shear rate,[38] as well as recording the dynamical change in the rheological parameters under dewatering.[40,41] To prevent evaporation of the water medium, a layer of silicone oil was spread over the surface of the sample in contact with the air, a common procedure.[31] By monitoring the viscoelastic moduli prior and after each experiment, we checked that evaporation or chemical aging of the sample was negligible.

We note that the adopted parallel-plate geometry is very prone to shear inhomogeneities, such as shear banding due to the inherent shear gradient in the radial direction.[42] This is especially true for shear-thinning complex fluids, such as coating colors. Furthermore, because we later discuss dewatering, it is well documented in the literature that vacuum filtration induces a gradient in the solid content in the filter normal direction.[43] However, to provide a uniform thickness of color during dewatering, a main target of the study, the parallel-plate geometry is an absolute given. Therefore, all of the rheological properties of the samples measured in this way correspond to their apparent values specific for this geometry and are suitable only for comparative purposes. Rheograms are made from representative measurements, and for calculation of the rheological parameter, average values of five measurements are used.

Viscoelastic Behavior. Dynamic moduli, storage modulus (G') and loss modulus (G''), were measured as a function of the angular frequency (ω = 0.1−100 s^{-1}) using oscillatory tests. To perform the frequency sweep test, the LVE range of the sample was obtained from an amplitude sweep using a constant angular frequency (ω = 1 s^{-1}) with varying strain amplitude between 0.01 and 500%.

Apparent Extrapolated Yield Stress. For a flow property comparison of different MFC/NFC suspensions, we fitted data of steady-state flow from shear range flow curves for an increasing upward shear rate range of 0.001−1000 s^{-1} as applied in the Herschel−Bulkley equation to obtain the apparent yield stress,[44,45] given by

$$\tau = \tau_0 + K(\dot{\gamma})^n \quad (1)$$

where τ is the shear stress, τ_0 is the apparent yield stress, K is a constant, termed consistency, $\dot{\gamma}$ is the shear rate, and n is the fluid index describing the flow behavior in an assumed power law. MFC/NFC suspensions are well-known to exhibit large rheological hysteresis;[46−48] therefore, it is advisable to perform a complete reverse sweep cycle (up and down in the shear rate) in order to exclude data from any likely shear banding area, which, as mentioned before, may occur under the parallel plate−plate geometry.[49] For determination of the local yield stress, we used the shear stress value generated after shear at 20 and 500 s^{-1}, respectively, in which regions are seen to be linear profiles after the curve bending area as a function of the change of the shear rate.[15]

Shear-Thinning Behavior. Shear thinning is clearly observable in the rheological response behavior discussed above. In

dx.doi.org/10.1021/ie4028878 | Ind. Eng. Chem. Res. 2013, 52, 16066−16083

this section, we investigate the shear-thinning nature using a variety of shear application devices, interpreting the various expressions of viscosity in order to derive likely structural behavior during the shear-thinning process. This is important for the early stages of dynamic dewatering before the increasing elastic component defines the immobilization state.

Apparent Viscosity under Low Shear "Stirring". The static apparent viscosities of MFC and NFC suspensions at 1.5% consistency were measured with a Brookfield viscometer (Brookfield DV-II) adopting a vane v-73 for MFC and v-74 for NFC viscosity units at a rotation speed of 10 min^{-1}. The apparent low shear (stirring) viscosity of the coating colors was determined also using the Brookfield viscometer operated respectively at two rotation speeds, 50 and 100 min^{-1}, with spindle #4 chosen in this case. For each measurement, a new sample was used, and the mean values of the last five data points at a given rotation speed were used for analysis of the experimental data. All measurements were performed at room temperature. Data from apparent low shear viscosities are presented in Table 2.

Dynamic Viscosity from a Steady-State Flow Curve. The influence of the shear rate on the variation of the dynamic viscosity was observed by measuring the steady-state flow curve using an increasing shear rate in the range 0.001−1000 s^{-1}, with data point duration 10 s. The influence of the shear rate on the variation of the complex viscosity was evaluated by measuring the complex viscosity response as a function of increasing oscillation frequency (angular frequency ω = 0.1−100 s^{-1}). A power law according to the Oswald de Waele empirical model was fitted to the experimental data for both the dynamic and complex viscosities (eq 2), allowing a comparison of the power law coefficients between the different deformation rates and conditions, i.e., within the local linear viscoelastic (LVE) region for the complex viscosity and beyond the elastic region for the dynamic viscosity, respectively[34,50,51]

$$\eta = k\dot{\gamma}^{-n} \tag{2}$$

where η is the viscosity, $\dot{\gamma}$ is the shear rate, and k and n are the flow index and the power law exponent, respectively. Here n = 0 indicates a Newtonian fluid and n > 0 pseudoplastic (shear-thinning) behavior.

Leveling and Recovery 3ITT Measurements. Leveling and recovery measurements were performed with the help of the three-interval test (3ITT test).[35,36] Two different 3ITT tests were performed: rotational and elasticity recovery tests.

To evaluate the evolution of the dynamic viscosity (η) after high shear stress, the *3ITT rotational test* was performed consisting of a stepwise shear rate test with three defined intervals of applied shear: low shear interval/high shear interval/low shear interval.[36] During the first and third intervals, the sample was sheared at a low shear rate of 0.1 s^{-1}, while the second interval was with a high rotation rate of 500 s^{-1}. This measurement shows the deformation and recovery of the structure through regeneration of the dynamic viscosity; i.e., how fast coating colors can regenerate the viscosity after application of a high shear period or impulse. Structure recovery was traced with respect to the time needed for a given coating color to recover 90% of its dynamic viscosity value before deformation (at the end of first interval).

In order to evaluate the evolution of the elastic modulus after the application of high shear, a *3ITT elasticity recovery* test was made, consisting of three intervals: oscillation/rotation/

Table 2. Results of Low Shear Apparent Viscosity (Brookfield) and Gravimetric Dewatering (ÅA-GWR) for MFC/NFC and Coating Colors[a]

	MFC	NFC	cGCC/CMC	cGCC/MFC	cGCC/NFC	fGCC/CMC	fGCC/MFC	fGCC/NFC	75 cGCC/ref	75 cGCC/MFC	75 cGCC/NFC	50 cGCC/ref	50 cGCC/MFC	50 cGCC/NFC	100 clay/ref	100 clay/MFC	100 clay/NFC
consistency (%)	1.5	1.5	63	63	63	63	63	63	63	63	63	63	63	63	63	63	63
AA-GWR($g \cdot m^{-2}$)	1132	219	198	235	213	189	233	208	153	190	195	99	194	206	129	152	194
Brookfield/10 min^{-1} (mPa·s)	151768	74334															
Brookfield/50 min^{-1} (mPa·s)	53268	16345	844	534	793	1809	1459	1548	896	525	652	782	480	581	725	330	423
Brookfield/100 min^{-1} (mPa·s)	33666	9987	512	328	496	1 094	894	981	553	339	422	476	307	374	431	225	275

[a]Complementary to the GCC portion is the kaolin (clay) in all clay-containing formulations in order to form 100 pph pigment.

dx.doi.org/10.1021/ie4028878 | Ind. Eng. Chem. Res. 2013, 52, 16066−16083

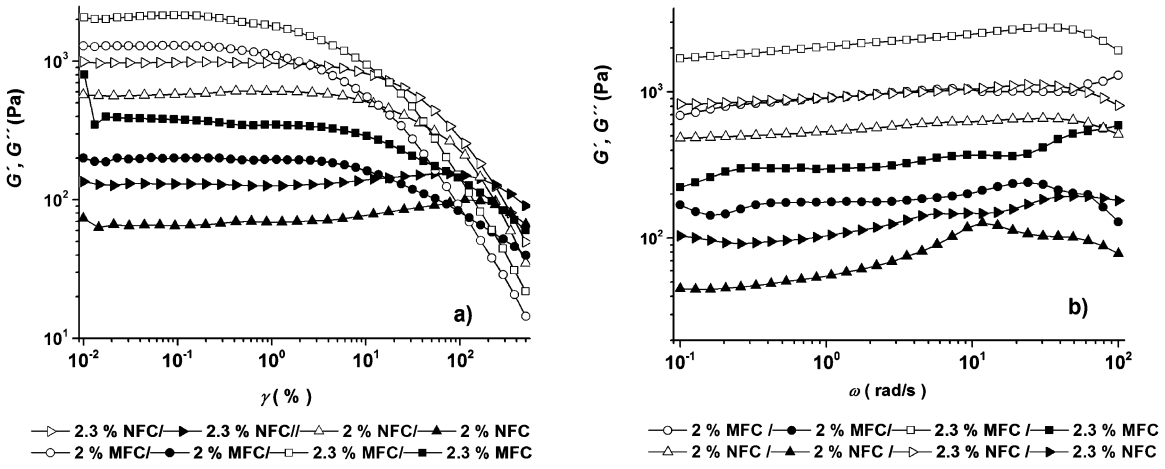

Figure 1. Viscoelastic measurements for MFC and NFC suspensions at 2% and 2.3% consistency: (a) amplitude sweep for a range of strains (γ = 0.01−500%) at a constant angular frequency of 1 rad·s^{-1}; (b) frequency sweep (0.1−100 rad·s^{-1}) at a constant strain of 0.1%. Open symbols: elastic modulus (G'). Closed symbols: loss modulus (G'').

oscillation.[35] In the first interval of oscillation, the test was performed at constant angular frequency [constant direct strain oscillation (DSO)] ω = 10 s^{-1} and strain γ = 0.01%, which has a value in the LVE range determined previously by an amplitude sweep test. During the second interval, a deformation was applied to the sample under a rotational regime with a high shear rate of 500 s^{-1}. The time taken for the structure to be regained to 90% of the G' value it had prior to the high shear interval was evaluated as an indication of the thixotropic behavior of the material. It should be noted here that complex systems, as described by the materials used in this study, i.e., nanofibrillar and micro- and macrofibrous as well as colloidal particulates, undergo multiple structural configurations including, and generating, a variety of elastic interactions. The elastic behavior is, thus, dependent on the material particulate and colloidal configurations, and so for each interaction, or combinations of interactions, there exists a localized elastic regime dependent on the strain rate condition applied. Thus, the term LVE in this context refers to the particular LVE region applicable for the fixed frequency of oscillation used.

Gravimetric Dewatering ÅA-GWR. The static gravimetric dewatering of coating colors was measured using the Åbo Akademi Gravimetric Water Retention device (ÅA-GWR).[52] A volume of 10 cm^3 of coating color was inserted into the cylindrical vessel above a polycarbonate membrane (Nucleopore Track-Etch membrane 5 μm, Whatman) and an absorbent blotter paper. The cylinder was closed and the sample held under an overpressure of 0.5 bar. After 1 min and 45 s, during which dewatering through the membrane occurred, the pressure cylinder was removed. The blotter paper was weighed before measurement and 30 s after the pressure was released. The weight difference was multiplied by 15091 m^{-2}, which is the inverse of the cylinder cross-sectional area. An average of five determinations was computed.

Dynamic Dewatering Measurements. Dynamic dewatering measurements under continuous shear were performed using a dewatering unit with a parallel-plate geometry (the immobilization cell, IMC).[41,43] The parallel plate of 50 mm diameter (PP-50) was adopted in all immobilization tests. The initial gap was set to 1 mm. The filter medium used in these experiments was a hydrophobic Whatman Nucleopore membrane, with a pore size of 0.2 μm. In the experiments, the temperature was kept at 23 °C and the preset shear rate was 100 s^{-1} applied for 40 s. We chose a testing approach in which the sample is subjected to DSO within the LVE range. The method as described is reported also by other authors,[41] and the procedure is designed to provide dynamic rheological information for a viscoelastic material during dewatering on the IMC apparatus. The oscillatory parameters during the measurement were γ = 1% and ω = 10 s^{-1}. The transition from liquidlike to solidlike behavior for a viscoelastic coating material during immobilization has been described as the maximum slope of the loss factor, which is the ratio of the viscous to elastic moduli, G''/G' = tan δ.[18,41] In the DSO test, during the progressive transition between liquidlike to solidlike behavior, the loss factor decreases with increasing time, reaching a minimum with $G' > G''$.

During dewatering in the IMC, the structure of the sample evolves as the solid content increases. The volume of the sample decreases, which is reflected by an artificial reduction in the normal force as soon as the vacuum $|-\Delta p|$ = 40 kPa is initiated (under pressure conditions similar to those in gravimetric dewatering measurements). After the automatic gap setting is applied, the normal force should remain zero, and the measuring system thus compensates for its negative values, which appear as a result of a tensile stress developing with dewatering.[43] The measuring instrument tries, therefore, to compensate for the negative normal force by moving the upper plate to decrease the gap. Thus, the gap becomes smaller as a result of the normal force decrease (i.e., the solid content increase leads to a reduced sample thickness). In fact, if the sample could be measured at constant volume, as the solid content increases, so would the normal force because of the increase in the elasticity.

Immobilization Solids. In order to investigate the immobilization layer further, the material that remained on the upper plate after it had been lifted up at the end of the dewatering tests was scraped off and analyzed gravimetrically, as described in previous research. The height of the apparent filter cake, determined by using the rheometer gap height, as was followed by other authors,[43] was not studied because we considered that, because of gel-related viscoelastic effects that might arise during formation of a concentration gradient upon vacuum dewatering of MFC/NFC-based coatings, the definition of a mechanically formed static filter cake per se is questionable.[34]

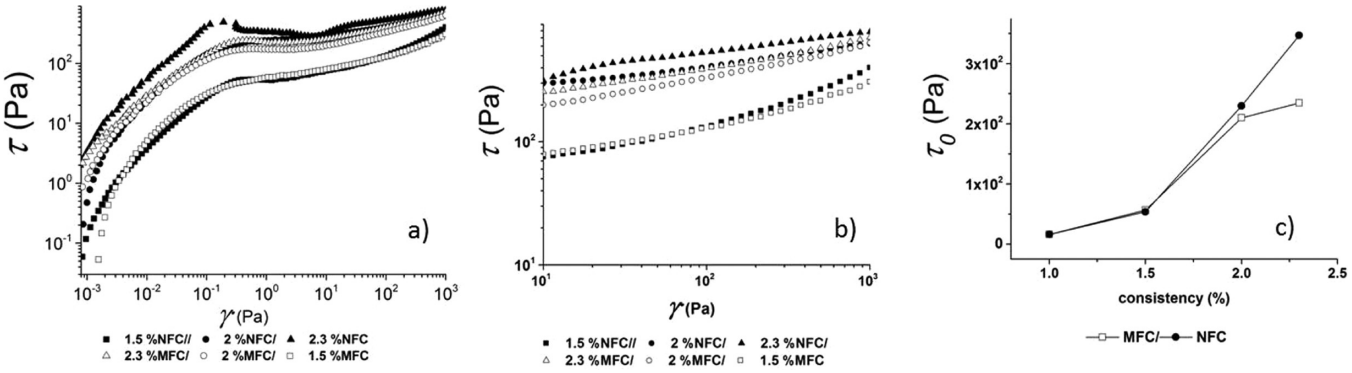

Figure 2. Steady-state flow curves for MFC/NFC suspensions for shear rate ($\dot{\gamma}$ = 0.001−1000 s^{-1}), time between points 10 s: (a) shear stress (τ) against shear strain (γ) over the whole shear rate range; (b) shear rate region for determination of the apparent yield stress (τ_0); (c) apparent yield stress (τ_0) for MFC/NFC suspensions as a function of the consistency.

RESULTS AND DISCUSSION

Rheological Characterization. *Low Shear Apparent Viscosities.* As seen in Table 2, a low shear apparent viscosity (Brookfield) at 10 min^{-1} is higher for MFC than for NFC suspensions, probably because of greater entanglement of the retained swollen fibrous material in the MFC.[14]

A comparison of the apparent viscosity values from the coating colors at rotation rates of 50 and 100 min^{-1} shows that, across the formulated coating colors, for each given pigment blend CMC as the cobinder always gives a higher viscosity value than MFC/NFC as the cobinder, which can be associated with the induced flocculation mechanism between CMC and pigments/latex.[27,53] The higher mobility of the particulates in the MFC and NFC coating color matrix is reflected in a lower viscosity value. Contrary to the MFC/NFC suspensions, coating colors with NFC as the cobinder have higher apparent viscosity than those with MFC, which is considered to be related to the independent structural behavior of MFC and pigment, with the pigment effectively acting to dilute the fibrous component and so partially inhibit the fiber entanglement seen with MFC alone.[54]

Viscoelastic Behavior of MFC/NFC Suspensions. The MFC and NFC suspensions exhibit linear viscoelastic responses at low strain. Parts a and b of Figure 1 show that within the LVE regime, below critical strain γ_c, MFC suspensions have higher elastic (G') and loss (G'') moduli than NFC suspensions at the same consistencies. This correlates well with the Brookfield findings above. Figure 1a shows that the LVE region is further extended for NFC suspensions (with the critical strain for MFC suspensions being $\gamma_c \sim 0.015\%$, and that for NFC suspensions $\gamma_c \sim 0.8\%$) because of a stronger gel-like structure typical for NFC suspensions at concentration higher than 1%, which is seen in the flow curve as an elastic overshoot, being highest for the 2.3% NFC suspension.[46] For both MFC and NFC suspensions, the storage modulus (G') is much greater than the loss modulus (G''), which indicates a solidlike elastic behavior of the material typical for a gel-like structure. The same indication of entanglement versus gel-like structure is depicited in Figure 1b, with viscoelastic moduli (G' and G'') for the MFC suspensions being higher than those for the NFC suspensions. Lower G' and G'' for NFC suspensions, which have higher ζ potential, reflecting greater surface charge, have been observed before.[55,56] This is due to the higher surface charge acting to decrease friction due to both the charge repulsion and a more spherical presentation to flow, thus increasing the mobility radius within the suspension matrix. In contrast, the likelihood of flocculation and entanglement in the MFC suspension is greater. Elastic moduli G' show an independence of frequency, but the viscous moduli G'' show a slight increase toward higher frequency, with the loss factor ($\tan \delta$) being around 0.2, again giving the indication of gel-like structures. Similar behavior is observed for MFC/NFC suspensions at 1% and 1.5% consistencies.

The steady shear behavior for MFC/NFC suspensions at increasing shear rate over the range 0.001−1000 s^{-1} (Figure 2a) is used for determination of the dynamic apparent yield stress using the Herschel−Bulkley equation (1), as shown in Figure 2b.

The Herschel−Bulkley equation does not apply very well across the whole shear stress profile because of the elastic overshoots typical for MFC/NFC material, which have high elasticity,[42] apparent in the steady shear measurements, which have short measurement time (Figure 2a), as observed by other researchers.[42,49] Therefore, we obtained an apparent dynamic yield point by analyzing the data at shear rates higher than the transition area, i.e., in the shear rate region between 20 and 500 s^{-1}, following the procedure described by Karppinen et al.[15] (Figure 2b). As expected, for all solids, the yield stress increases with an increase in the suspension consistency, as was also observed before by other authors.[50,51] At lower consistency, the yield stress is almost the same for MFC and NFC suspensions, increasing for NFC for consistencies higher than 1.5% because of the inhibited hydrogen bonding of higher-specific-surface-area NFC (Figure 2c), which gives rise to gel-like structures, seen as elastic overshoots in the flow curve for the 2.3% NFC suspension.[46] Apparent yield point values are for 1% MFC, 43 Pa, and for 1% NFC, 50 Pa; for 1.5% MFC, 60 Pa, and for 1.5% NFC, 62 Pa; for 2% NFC, 194 Pa, and for 2% NFC, 230 Pa; for 2.3% MFC, 218 Pa, and for 2.3% NFC, 347 Pa.

Because of the necessity of extrapolating to the apparent yield stress point using the Herschel−Bulkley expression over a range where the power law behavior dominates, i.e., beyond the structure transition in the increasing shear rate regime, clearly it is not possible to define the static rest state yield. However, adopting this technique, we believe, provides a better description of the approach to immobilization under dynamic dewatering, i.e., while being sheared. The apparent yield stress is then greater (Figure 2c) than the stress seen at low shear (Figure 2a). We consider this to be an indication of the greater dispersed nature of NFC/MFC under shear and so the longer

dx.doi.org/10.1021/ie4028878 | Ind. Eng. Chem. Res. 2013, 52, 16066−16083

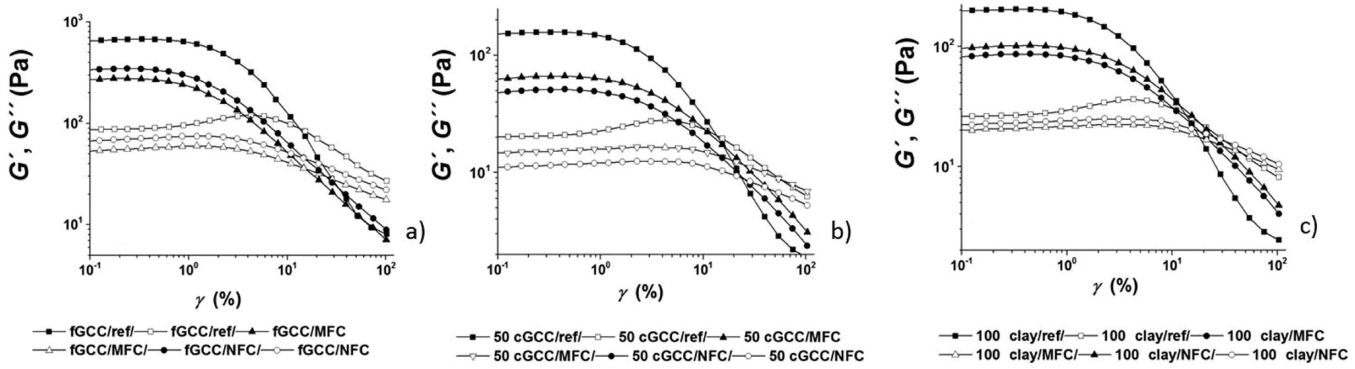

Figure 3. Storage (G') and elastic (G'') moduli against strain (γ) for the various coating color thickener systems containing (a) fGCC, (b) 50:50 cGCC/clay, and (c) 100 clay. Complementary to the GCC portion is kaolin (clay) in all blend formulations in order to form 100 pph pigment. Closed symbols: elastic modulus (G'). Open symbols: loss modulus (G'').

range likelihood of gel formation when fibrils are effectively uncoiled.

Nonlinear Viscoelastic Behavior of Coating Colors. Oscillatory measurements were used to characterize the microstructure of the coating colors.[30,35,39] Parts a–c of Figure 3 illustrate the storage (G') and loss (G'') moduli as a function of the strain at a constant angular frequency of 1 Hz. The elastic modulus is constant up to a critical strain γ_c (~0.015%), above which the storage modulus decreases with strain and the viscoelastic behavior becomes nonlinear. Therefore, outside the LVE region, the elastic and viscous moduli values can only be considered as apparent values. Figure 3 reports the storage and loss moduli as a function of the strain amplitude for fGCC and the two clay-containing coatings, with the three different cobinder systems. The first observation is that, for all coatings, the presented G' is much larger than G''. Second, G' values are larger for the CMC-only reference coatings than those having fibrillar/nanocellulose as the cobinder. The linear domain, in which the storage modulus G' is limited to a value of 95% of that of the plateau value[30,57] is extended further with respect to shear stress for kaolin coatings than for carbonate coatings because of stronger supramolecular structure buildup by CMC and kaolin.[27,32] It is common here, regardless of the pigment type, that a transition between the linear and nonlinear regimes occurs at larger deformations when nanocellulose is included in the cobinder system, indicating that a potentially different thickening mechanism is at play.

In Figure 4a–e, the G' and G'' moduli in the linear regime are presented as functions of the frequency. Again we notice that G' is considerably larger than G'', and G' increases slowly with the frequency, while its magnitude remains considerably larger than that of G'', as has been observed by other authors. The G'' increase at higher frequencies and the slight G'' decrease at lower frequencies has also been observed by other authors.[31,39]

The variations in the viscoelastic moduli, with respect to the proportion of pigment types in the coating color formulations and cobinder type, are plotted in Figure 5, with G' and G'' values at γ = 0.2 (%) taken from the angular frequency sweep measurement.

For coating colors that have kaolin pigments, G' and G'' in Figure 5 both increase with an increase in the proportion of kaolin in the pigment coating formulation blend. For coatings without kaolin pigment, G' and G'' increase with higher pigment packing density, similar to that seen for the apparent viscosity. The flocculation mechanism of CMC on pigments has been studied before,[23,27,29,58] and it is observed that formation of the floc structures, formed in this way, increases the elastic component in the coating rheology. However, all coatings show a decrease in elastic moduli when CMC is partially replaced with nanocellulose. The decrease in G' can be explained through reduced interaction with the thickener system as the amount of CMC is reduced in relation to the pigments/latex. That the replacement of CMC by cellulose does not regenerate the floc structure interactions shows that the pigments/latex and NFC essentially behave more or less independently in the mixed environment. This may be due to their mutual charge repulsion and/or the higher interparticle mobility of swollen nanocellulose,[50,59] which results in lower elasticity than in the case of the higher CMC level in the presence of pigments/latex.[27,29,32] Solidlike behavior of coatings under the blade occurs if the deformation time is very short compared to the relaxation time. It is noted that using very low rates of change of strain, as applied here during oscillation measurements, is very different from the high rates of change of the shear rate conditions under a coating blade, but it is likely that the underlying elasticity is, nonetheless, identifiable because breakdown of most of the color structure is only likely to occur in practice if the time scale is long enough at high strain, i.e., under pumping rather than during the short residence time under the blade.[16,25]

Shear-Thinning Behavior. Shear thinning is clearly observable in the rheological response behavior discussed above. In this section, we investigate the shear-thinning nature using a variety of shear application devices, interpreting the various expressions of viscosity in order to derive likely structural behavior during the shear-thinning process. This is important for the early stages of dynamic dewatering before the increasing elastic component defines the immobilization state.

Complex Viscosity. The complex viscosity is obtained from frequency sweep tests, and its shear-thinning response within the local LVE region as the frequency of oscillation increases helps to characterize the rheological properties of the suspension. The reduction in the complex viscosity (η^*) under increasing shear rate characterizes the transition from elastic to viscous behavior, and thus at highest shear, the inability to rebuild the structure in the time period of the applied oscillation, or, as is commonly considered, the resistance to viscosity change during deformation, is observed.[16,23] The absence of a further induced elastic structure at the higher frequency range supports the noninteractive nature of nanocellulose with the particulate materials present.

dx.doi.org/10.1021/ie4028878 | Ind. Eng. Chem. Res. 2013, 52, 16066–16083

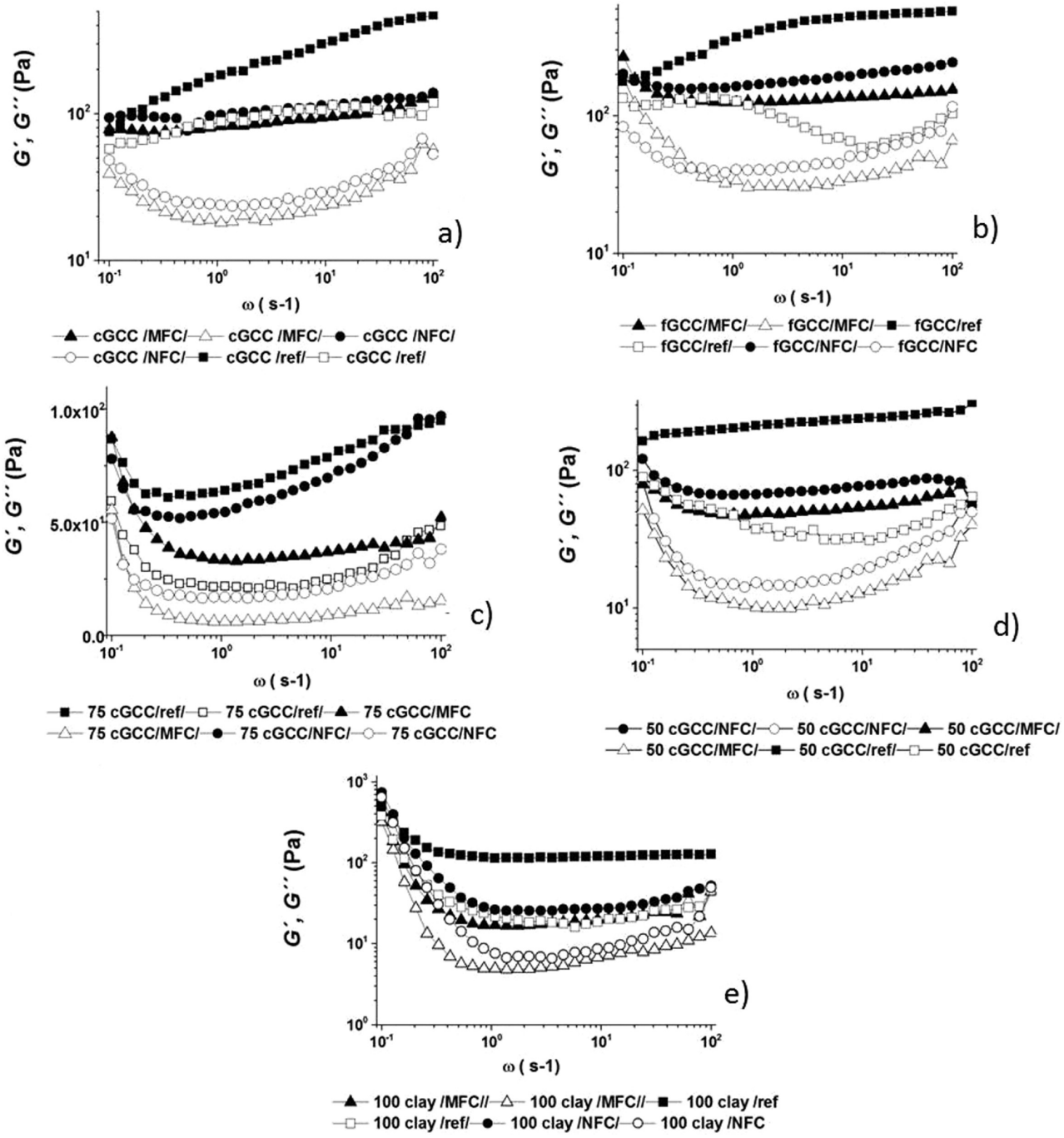

Figure 4. Responses of G' and G'' against frequency (ω = 0.1−100 rad·s^{-1}) for all coating colors: (a) 100 cGCC; (b) 100 fGCC; (c) 75 cGCC; (d) 50 cGCC; (e) 100 clay. Complementary to the GCC portion is kaolin (clay) in all formulations in order to form 100 pph pigment. Closed symbols: elastic modulus (G'). Open symbols: loss modulus (G'').

Table 3 shows the complex viscosity response (η^*) for all coatings as defining the major difference between CMC- and MFC/NFC-containing cobinder systems. Figure 6a shows the complex viscosity (η^*) over the whole frequency range (ω = 0.1−100 rad·s^{-1}), for 50 cGCC coatings; similar behavior is observed for all other coatings and presented in Table 3.

Dynamic Viscosity, Nonlinear Tests. Steady shear flow curves of coating colors are presented in Figure 6b. All coatings show a similar pattern of a decrease in the viscosity as the shear rate (γ) increases from very low to very high (γ = 0.001−1000 s^{-1}), i.e., shear-thinning behavior. Unlike in the case of complex viscosity, where elucidation of the elastic and viscous components is combined under oscillation, the dynamic flow curves show three distinct regions.[31,57]

We defined the three distinct areas in the flow curves covering three shear zones: (1) γ = 0.001−100 s^{-1}, over which the viscosity decreases drastically and data do not follow a single power law behavior; (2) at shear rates γ = 100−500 s^{-1}, in which all flow curves follow a close fit to a perfect power law behavior; (3) at high shear rates γ = 500−1000 s^{-1}. It is important to point out that in the shear zone with the highest shear rate NFC coatings have a further strong drop in viscosity at very high shear rates because of either a complete collapse of the gel-like structure within the coating color matrix or, much

dx.doi.org/10.1021/ie4028878 | Ind. Eng. Chem. Res. 2013, 52, 16066−16083

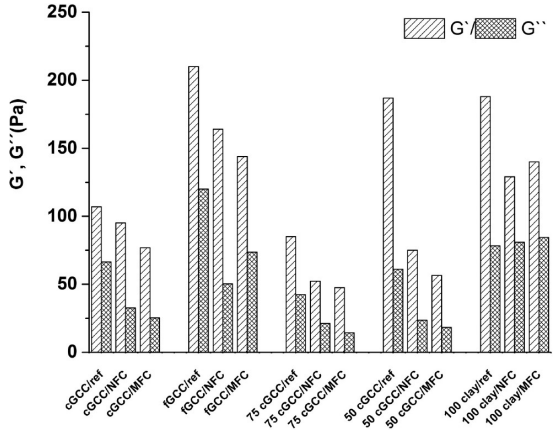

Figure 5. G' and G'' for coating colors during the angular frequency sweep, taken at $\omega = 0.2$ rad·s^{-1}. Complementary to the GCC portion is kaolin (clay) in all blend formulations in order to form 100 pph pigment.

more likely, the establishment of a boundary slip condition due to the expulsion of water from the gel, as presented in Figure 6b. This latter effect, if confirmable, is potentially a vital observation with respect to blade coater runnability and the establishment of plug flow under a high-speed running blade.[16,25,31]

Fibrillar Coiling: Cox–Merz Rule? For most systems, particularly polymers, the complex viscosity (η^*) provides a convenient measure of the structural components contributing to low shear viscosity. If the dynamic shear response behavior against the shear rate is the same as the complex response as a function of the frequency, i.e. when expressed in the two forms, then one can derive a polymer-like behavior according to the Cox–Merz empirical rule.[60] This behavior in pure polymer solutions reflects the structural state of the polymer transitioning from a coiled configuration to that of an extended linear array. Figure 6c shows clearly that the Cox–Merz rule does not hold for MFC/NFC coating colors, with the complex viscosity being much higher than the dynamic viscosity, and this follows observed behavior for MFC/NFC suspensions reported by other authors.[51] We speculate once again that this relates to the binding of water within a gel structure rather than the more simple uncoiling and alignment behavior of microfibers that are not so water binding and so normally express their aspect ratio more definitely under both oscillatory strain and dynamic shear.

Power Law Behavior of Flow Curves. In order to compare the different responses of complex (η^*) and dynamic viscosity (η) of the coating colors, we use iterative least-squares methods to calculate an average value of the shear-thinning coefficient (n) for each of the flow curves at a given viscosity (η and η^*) and observe the behavior of the flow coefficient k for the complex and dynamic viscosities, respectively, as in eq 2. The flow coefficients (k) for complex viscosities (η^*) for the given fitted shear-thinning index ($n = 0.82$) are presented in Table 3. We see in most cases that k is larger for NFC-containing than for MFC-containing coatings, indicating the strong gelation properties of NFC and/or theoretically the flocculation of pigment. These findings correlate with the Brookfield results. That this is occurring to a lesser degree in the presence of MFC supports the option of the dominance of gel formation in the NFC case because NFC would have a far greater number frequency of occupation in floc-related structures if the pigment were to be strongly flocculated by NFC, and clearly this is not

Table 3. Shear-Thinning Behavior for All Coating Colors: Initial and Final Values of Flow Curves for Complex Viscosity Response (η^*) and Dynamic Viscosity (η) with Their Respective Fitted Flow Indices (k) and Shear-Thinning Coefficients (n)

	cGCC/CMC	cGCC/MFC	cGCC/NFC	fGCC/CMC	fGCC/MFC	fGCC/NFC	75 cGCC/ref	75 cGCC/MFC	75 cGCC/NFC	50 GCC/ref	50 cGCC/MFC	50 cGCC/NFC	100 clay/ref	100 clay/MFC	100 clay/NFC
η^* (Pa·s) at $\omega = 0.1$ rad·s^{-1}	1 157	978	1 060	2 870	1 790	2 180	1 380	949	1 270	1 181	1 040	1 048	2 490	5 000	6 810
η^* (Pa·s) at $\omega = 100$ rad·s^{-1}	1.47	1.45	1.49	2.90	1.35	2.70	1.96	0.74	1.09	1.38	0.60	0.82	1.58	0.56	0.71
η (Pa·s) at $\dot{\gamma} = 0.01$ s^{-1}	378	252	206	252	245	214	157	344	254	154	335	252	166	344	274
η (Pa·s) at $\dot{\gamma} = 100$ s^{-1}	0.280	0.290	0.150	0.287	0.317	0.150	0.198	0.247	0.280	0.190	0.241	0.287	0.210	0.250	0.310
η (Pa·s) at $\dot{\gamma} = 1\,000$ s^{-1}	0.050	0.040	0.020	0.040	0.050	0.20	0.040	0.450	0.030	0.030	0.440	0.040	0.040	0.050	0.040
k_{η^*} ($n_{\eta^*} = 0.83$)	181.2	63.4	69.3	262.2	68.9	120.8	103.4	36.1	49.1	63.7	23.8	37.8	69.0	20.6	24.8
n_{η^*} ($k_{\eta^*} = 79.61$)	0.630	0.880	0.863	0.630	0.880	0.860	0.770	1.015	0.940	0.880	1.110	1.000	0.862	1.134	1.090
k_η ($n_\eta = 0.82$)	13.3	17.5	7.0	12.8	13.4	7.2	9.3	11.2	12.9	9.0	12.8	11.8	9.9	11.0	11.2
n_η ($k_\eta = 11.45$)	0.790	0.740	0.930	0.800	0.780	0.913	0.865	0.817	0.802	0.860	0.820	0.800	0.850	0.780	0.820

dx.doi.org/10.1021/ie4028878 | *Ind. Eng. Chem. Res.* 2013, 52, 16066–16083

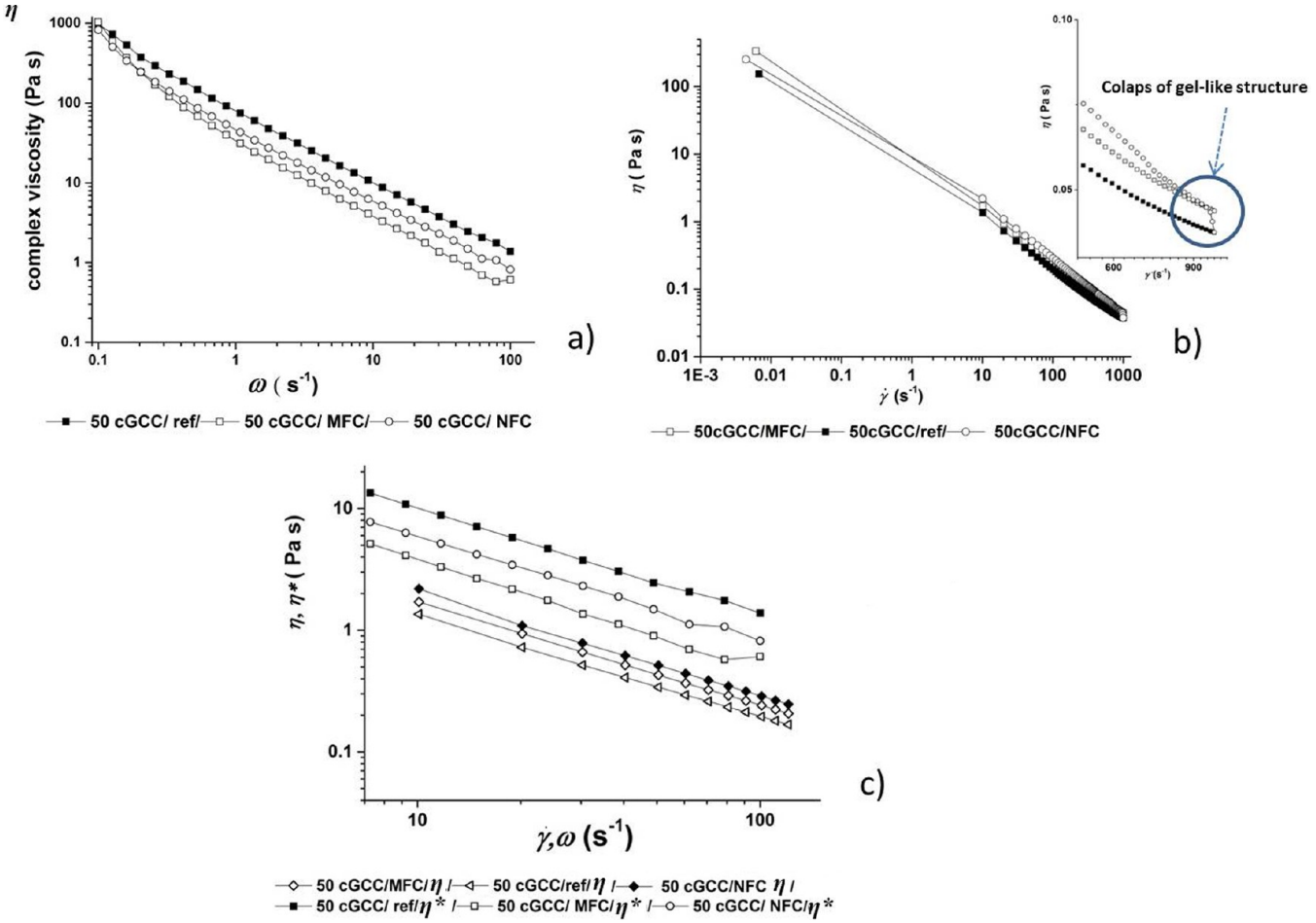

Figure 6. Shear-thinning behavior for representative coating 50 cGCC: (a) complex viscosity response (η^*) as a function of increasing frequency (ω = 0.1−100 rad·s^{-1}); (b) dynamic viscosity (η) as a function of the shear rate ($\dot{\gamma}$ = 0.001−1000 s^{-1}); (c) complex viscosity η^* (shown also as a sample label postscript) and steady-state viscosity η (shown also as a sample label postscript) as a function of the angular frequency and shear rate within the same range $\dot{\gamma}$ = 1−110 s^{-1} (Cox−Merz).

the mechanistic case. That the NFC system is not (or less) flocculated is supported in suspension by the higher repulsion between the anionic pigments and the high ζ potential of NFC, together with its enhanced gel state compared with MFC. The opposite is interestingly true for the dynamic viscosity case, where the k values are greater for the MFC-containing colors. This supports well the prediction that the retained fibers in MFC lead to an initial entanglement in the static state and become dispersed under dynamic shear.[46,47,50]

Structure Recovery Tests. So far, we have concentrated on the transition from the elastic static structure to high-strain or high-shear-rate breakdown of that structure. On the one hand, upon determination of the apparent yield stress of an otherwise sheared sample, using the Herschel−Bulkley model, eq 1, a measure of the likely final static structure could be derived from the structural state established under shear. Recovery, on the other hand, describes the reestablishment of the true static state after shearing as is set up prior to shear.

Rotational 3ITT. After coating color application by metering onto a substrate, the leveling and sagging are very important antagonistic properties that should, in turn, be maximized and minimized, respectively, for the final quality of the coating layer to be at an optimum. It is, therefore, desirable that the inner supraparticulate structure be regenerated within a certain time period before drying and before the coating holdout on the surface above the substrate voids is lost; i.e., leveling requires lower viscosity (slower regeneration), whereas sag prevention requires high viscosity (rapid regeneration).[35,36] Results from the viscosity recovery experiment 3ITT, with shearing over three intervals, go some way to elucidating this property balance. Initially, the samples are subjected to low shear rate, then subsequently high shear rate, and finally once again low shear rate "recovery". The high shear rate in the test reflects the shear rate during application. By this process, the structured entities break down, and their recovery to the preshear state in the postapplication of a high shear state can be measured. The most important aspect of the structure recovery test is determining how the change in the cobinder affects recovery of any network structure in the system after removal of high shear. The faster the increase (rebuild) of the viscosity, the better is the sagging resistance after application on a rough surface.[16,36] We note that sagging in the case of paint is usually gravity-driven, whereas in the case of paper coating, it is both drainage-flow-driven and, additionally, under capillarity. Too fast a recovery of viscosity can, on the contrary, affect leveling of the coating color after the blade because the shear stress for good leveling must be below the yield point.[36] Coating colors that have CMC as the cobinder have a typical overshoot behavior after high shear, which is more pronounced for kaolin-based coating colors because of the sudden loss of high-aspect-

dx.doi.org/10.1021/ie4028878 | Ind. Eng. Chem. Res. 2013, 52, 16066−16083

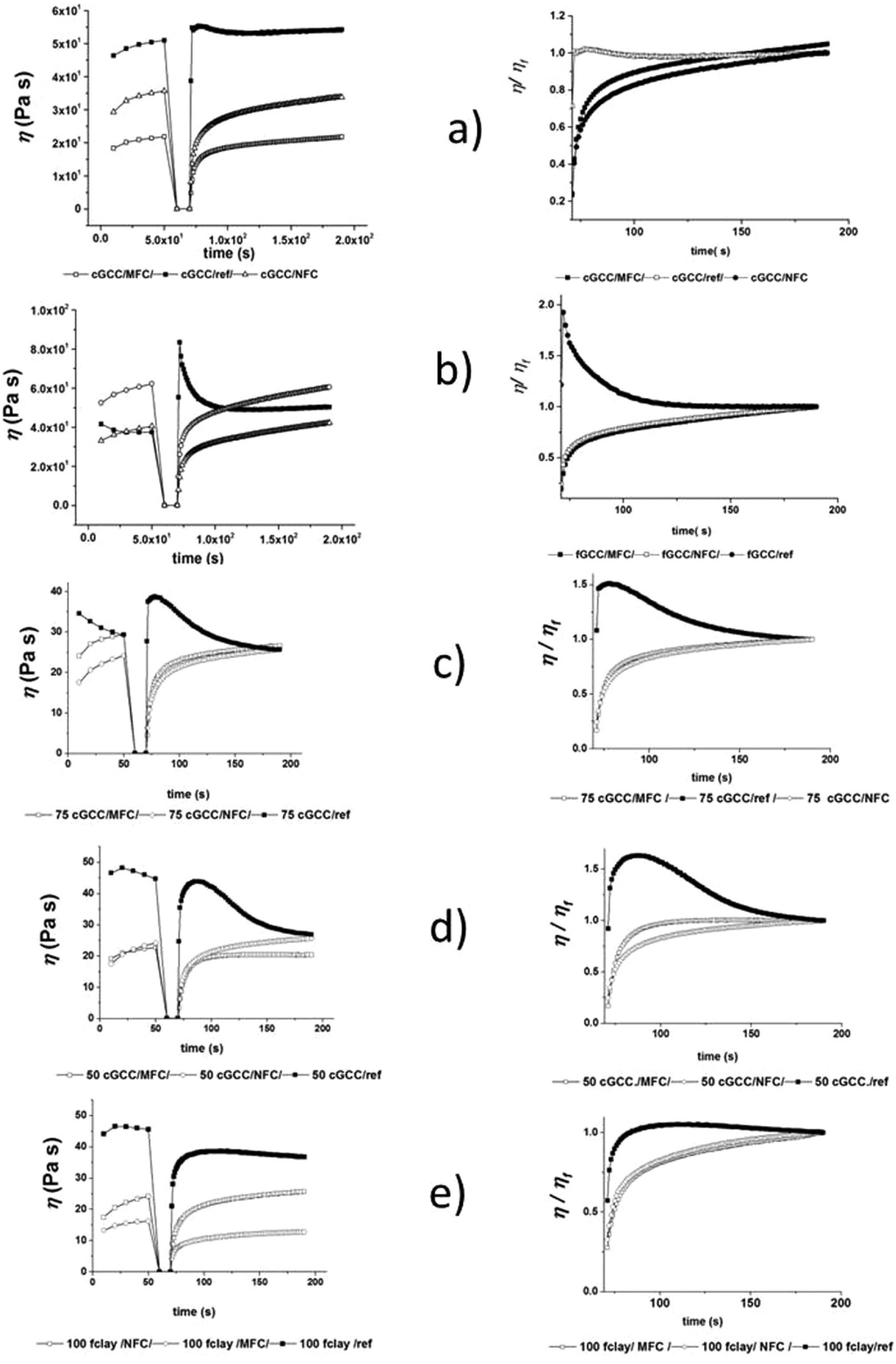

Figure 7. Dynamic viscosity (η) and normalized value (η/η_f) in the third interval of the 3ITT experiment with different shear: (a) cGCC; (b) fGCC; (c) 75 cGCC; (d) 50 cGCC; (e) 100 clay-based colors. Complementary to the GCC portion is kaolin (clay) in all blend formulations in order to form 100 pph pigment.

dx.doi.org/10.1021/ie4028878 | *Ind. Eng. Chem. Res.* 2013, 52, 16066−16083

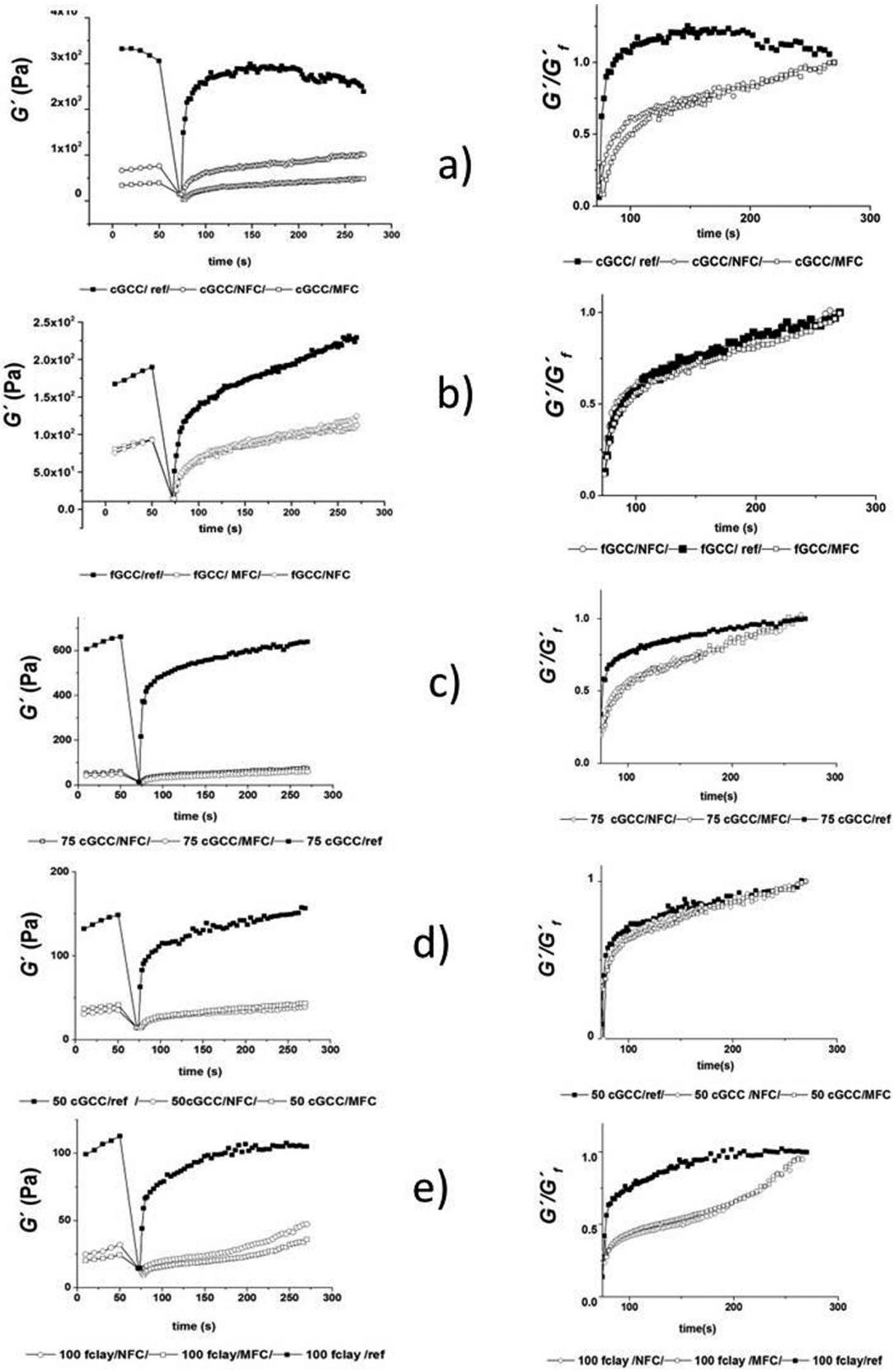

Figure 8. Elastic modulus (G') during the intervals oscillation/shear/oscillation in the 3ITT experiment and normalized elastic modulus (G'/G_f') after the third interval: (a) cGCC; (b) fGCC; (c) 75 cGCC; (d) 50 cGCC; (e) 100 clay formulations. Complementary to the GCC portion is kaolin (clay) in all blend formulations in order to form 100 pph pigment.

ratio particle alignment and the rapid reforming of the interaction between kaolin and CMC.[27,29] The overshooting behavior at cessation of high shear has been explained by other authors as being dependent on the type of CMC[27,32,61] and pH

dx.doi.org/10.1021/ie4028878 | Ind. Eng. Chem. Res. 2013, 52, 16066−16083

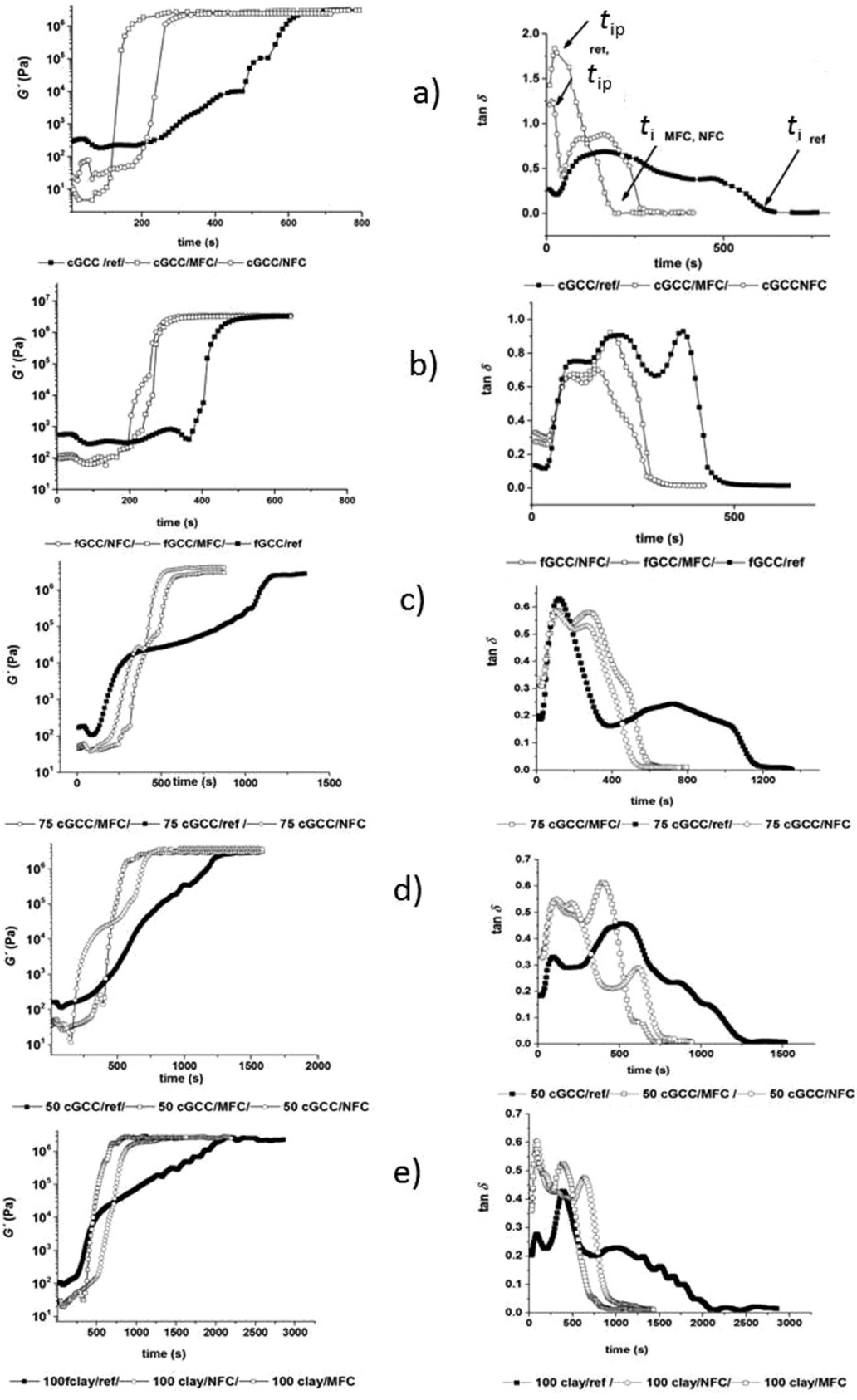

Figure 9. Elastic modulus (G') and damping factor (tan δ) immobilization rheograms: (a) cGCC; (b) fGCC; (c) 75 cGCC; (d) 50 cGCC; (e) 100 clay colors. Complementary to the GCC portion is kaolin (clay) in all blend formulations in order to form 100 pph pigment.

in the coating formulation and the pigment type. The viscosity increase in the third interval of the 3ITT test, normalized by its final value (η/η_f) at the end of the third interval, η_f, is presented on the left-hand side of Figure 7a–e.

dx.doi.org/10.1021/ie4028878 | *Ind. Eng. Chem. Res.* 2013, 52, 16066–16083

While the CMC coatings in the third interval show the expected overshooting character after high shear, described above, the behavior for MFC/NFC-containing coatings is very different because their viscosity after a very pronounced shear thinning at the transition to high shear increases the post high shear uniformly to reach equilibrium, without any overshooting character. Coating colors that have MFC/NFC as the cobinder show, in addition, slower viscosity "recovery" due to the free mobile nature of the movement between the nanocellulosic material and the pigments/latex. The observed results can be rationalized on the basis of the faster relaxation times associated with stronger polymer-induced interparticle interactions with CMC that cause faster structure recovery after disturbances during application. The patterns of the curves in Figure 7a−e show that after removal of the high shear rate the structure regeneration due to gel-network structure formation is slower initially for MFC/NFC-containing coatings because there is less interaction between MFC/NFC and pigments but rather slower diffusion-based capture of water to form a gel-network structure.

Elasticity Recovery: Oscillation 3ITT. The results from the 3ITT elasticity recovery test, with oscillation within the LVE region in the first and third intervals and high rotation in between, are presented in Figure 8a−e. Rheograms showing elasticity recovery (G') in the third interval after cessation of high stress illustrate the different structure recovery behaviors between CMC and MFC/NFC coatings, nicely supporting the interpretation of the data from the previous figures. The initial elasticity of CMC-containing coating colors in the LVE region is higher than that for MFC/NFC-containing coating colors, as discussed before, because of the viscoelastic character of the flocculation mechanism between CMC and pigments/latex, which is absent in the case of little or no direct interaction between the fibrillar MFC/NFC and pigments. Time-dependent elasticity recovery is also higher for CMC coatings, shown as a repeated pattern in the normalized elasticity (G' normalized by its final value G_f') diagrams (Figure 8a−e). The presence or absence of this mechanism affects the elastic response of viscoelastic coatings at the high rate of change of the shear rate under the blade.[16,29]

The overall conclusion of rotational and oscillatory 3ITT tests is that the traditional nature of interactivity induced by CMC with pigments/latex is very different from that of MFC/NFC and pigments and that CMC coatings will likely show somewhat worse leveling but better antisagging properties, which is an important parameter balance for coating coverage of rough substrates, whereas the increased mobility within the MFC/NFC gel structures will likely aid leveling on smooth substrates, such as when topcoating a precoated fine paper or multiprecoated boards.

Dynamic Dewatering with IMC. The dewatering rate is one of the most important factors controlling formation of the coating structure, which is manifest as retention of the immobilized state on the substrate surface.[16,43] The immobilization curves for the various coating colors are presented in Figure 9a−e in the form of the increase in G' during dynamic dewatering, i.e., dewatering under shear oscillation.[18,40,41] The data display clear differences in the rate and nature of dewatering, i.e., the increase in elasticity (G'). Carbonate-based coatings have less water retention properties than clay-containing coatings, with the coarse carbonate grade (cGCC) having the least water retention. The higher aspect ratio of clay is accountable, at least in part, for this, although the major effect with such high-aspect-ratio clay as used here is emphasized in the CMC−clay interaction[13,22] (Figure 9c−e). The finer carbonate grade (fGCC) has medium water retention in the series, related to the increased particle number (Figures 9a,b). Partial substitution of CMC with MFC/NFC decreases water retention because immobilization times decrease for all coatings regardless of the pigment blend, which is seen as a consistent pattern in all immobilization curves (Figure 9a−e). The immobilization curves of MFC/NFC-containing coatings have a much steeper increase in G', indicating much faster initial dewatering and lower retention over time, which could give rise to problems in applications where a too rapid water loss between the initial application and metering, connected also to potential binder migration and swelling-induced roughening of a base paper, can lead to runnability issues.[16,22] However, because it was seen in the 3ITT tests that sagging of MFC/NFC-containing coatings might be negatively influenced by the mobility of the particle flow, the more rapid immobilization could well compensate for or even improve on the coverage and antishrinkage properties. As reported from other research, dewatering in an IMC for traditional flocculation structure-based coating colors is characterized through changes in the loss factor $\tan \delta = G''/G'$,[41] as an indication of the relationship of the increase in viscous dissipation versus the increase in elasticity.[18] The start of immobilization is defined as the immobilization initiation point t_{ip}, indicating the onset of strong particle−particle crowding interactions over the maximum $\tan \delta$ range, while final immobilization, i.e., at immobilization time t_i, is the time when $\tan \delta$ reaches its plateau value.[41] Data presented on the left-hand side of Figure 9a−e) show the change in $\tan \delta$, indicating similar t_{ip} values for all coatings but differences in t_i between CMC-only and MFC/NFC-containing coating colors. Both cGCC and fGCC coatings having MFC/NFC as the cobinder (Figure 9a,b) have shorter t_i than clay-based MFC/NFC-containing coatings (Figure 9c−e). These shorter t_i observations for carbonate are seen to be similar to those for CMC alone in the coating mix but with a very different overall time scale; the difference in t_i between carbonate and clay when using MFC/NFC in the cobinder formulation is up to 500 s, while for CMC coatings, it is up to 1500 s. Given the previous rheological analyses, it is clear to see that this relates to the greater mobility in the MFC/NFC case versus the stronger differential flocculating effect between carbonate and clay in the presence of CMC.

To illustrate the link between structure recovery and dewatering, the structure regeneration of coating colors, as presented previously in Figure 8, was defined as the time needed for recovery to 90% of the viscosity/elasticity in the 3ITT tests.[36] The 90% recovery time in elasticity (G'), after removal of high shear/strain, was measured as an average of five measurements using values of normalized elasticity (G'/G_f) against time from Figure 8. As was also discussed previously, results from both the viscosity/elasticity 3ITT tests showed that the time-dependent structure regeneration after removal of the high shear rate, defined as recovery of viscosity and elasticity, is faster when CMC is used as the sole cobinder in the reference colors, indicating the stronger three-dimensional floc structure in comparison to the relative absence of interaction between the gel-like MFC/NFC and pigments, due to the repulsion mechanism between anionic particles and the water capture, especially of the finer highly swollen NFC.[16,29] The immobilization time (t_i) is defined as the time needed for $\tan \delta$ to reach its plateau, and the immobilization

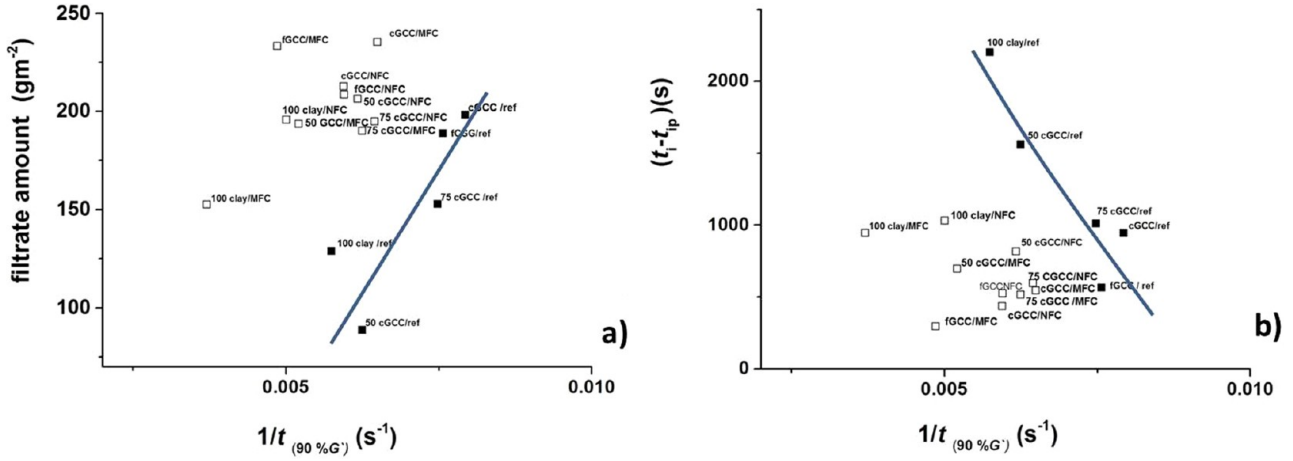

Figure 10. Influence of the coating color elasticity recovery on dewatering: (a) correlation among certain formulations between the filtrate amount with ÅA-GWR and the recovery value defined as the time needed for recovery of 90% of the starting elasticity (G') in the third interval of 3ITT tests; (b) correlation among certain formulations between the immobilization interval and the recovery value of the time needed for recovery of 90% elasticity (G') viscosity in the third interval of 3ITT tests.

interval ($t_i - t_{ip}$) as the time between the onset of immobilization, the immobilization initiation point (t_{ip}), and the final plateau of immobilization or end-point immobilization time. Here, we make a comparison between the filtrate amount under gravimetric dewatering and the immobilization interval with the elastic recovery property, as found in the 3ITT oscillation tests.

The correlation, therefore, between the filtrate amount and elasticity recovery presented in Figure 10a,b shows similar behavior for all CMC coatings, with higher structure elasticity indicating likely flocculation, which results in higher water retention under gravimetric dewatering for CMC coatings, as in Figure 10a, and longer immobilization intervals and faster elasticity recovery time, as seen in Figure 10b, as was already discussed in relation to Figures 7−9. In fact, the immobilization time behavior is seen to be much stronger in inverse correlation to the recovery in G' (Figure 10b), and this is logical because immobilization by definition means "reaching the point of an elastic solid".

To make the comparison, we use the simplified filtration model of the earlier stages of filtration based on Darcy's law, starting from the Hagen−Poiseuille equation, which gives the relation between the filtrate volume and time[62] as

$$\frac{dV}{dt} = \frac{\Delta P}{\eta(w\alpha_m V + r)} \quad (3)$$

where η is the filtrate viscosity, α_m is the specific mass filter cake resistance, w is the weight of cake solids per unit volume of filtrate, and r is the membrane resistance.

On the basis of the modified differential equation, which models the filtration behavior of compressed networked suspensions,[62] it has been proposed in other work on coating color dewatering and immobilization[40] that the following relation holds between gravimetric dewatering and immobilization interval

$$(V/A)_{WR} \sim \frac{1}{\sqrt{t_i - t_{ip}}} \quad (4)$$

where the $(V/A)_{WR}$ value is assumed to be the volume of the filtrate, V, per unit area A during the ÅA-GWR measurement and $t_i - t_{ip}$ the immobilization interval from the IMC tests defined above.

As we see in Figure 11, when CMC is partially substituted with NFC/MFC, the correlation in eq 4 does not convincingly

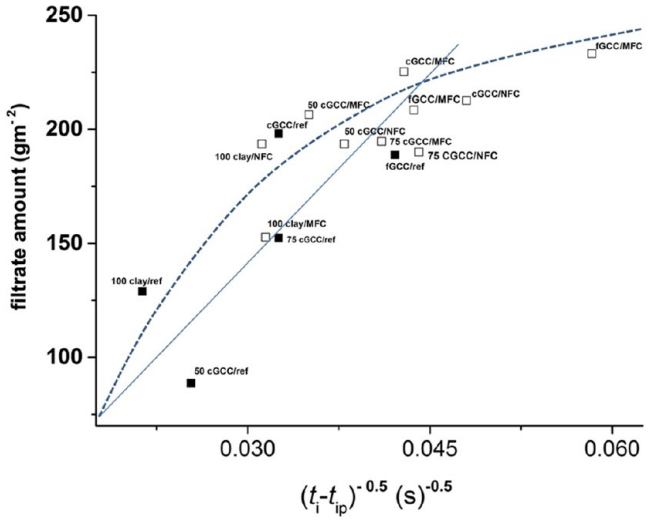

Figure 11. Correlation diagram showing the filtrate amount in the ÅA-GWR measurement and immobilization interval ($t_i - t_{ip}$) for reference and MFC/NFC coatings.

follow a linear trend except for the reference CMC as the sole cobinder samples but rather a curvilinear form encompassing the MFC/NFC-containing samples. We suspect that this is due to the difference in the mobility and interaction of pigment and CMC (flocculated in the combined structure) versus MFC/NFC (more independent behavior), related to the viscoelastic gel-like nature of MFC/NFC, which affects IMC measurements.[14]

For further investigation of the immobilized layer, the material remaining on the upper plate after it had been lifted up was scraped off and analyzed gravimetrically, according to the procedure described by previous workers. The resulting data are presented in Figure 12. Immobilization solids in the scraped-off portions showed slightly higher values for the MFC/NFC coatings. This, however, can only be considered as

dx.doi.org/10.1021/ie4028878 | Ind. Eng. Chem. Res. 2013, 52, 16066−16083

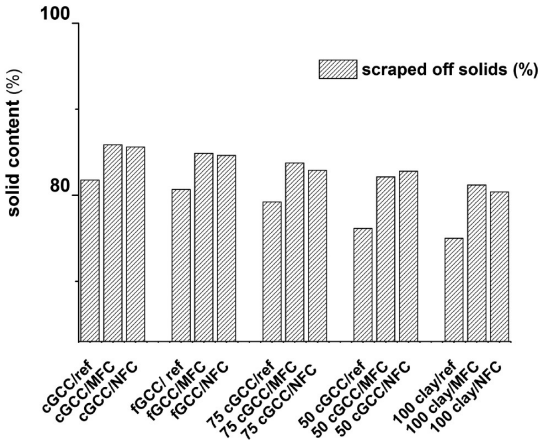

Figure 12. Solid content of an immobilized coating color sample obtained by the scrape-off method from the upper rheometer plate. Complementary to the GCC portion is kaolin (clay) in all blend formulations in order to form 100 pph pigment.

a rough method because there was a concentration gradient between the inner and outer parts of the immobilization layer, with the outer part being dryer than the inner, which is even more pronounced for rapid dewatering, as is the case with MFC/NFC-containing coatings. Nonetheless, the findings support the hypothesis of reduced interaction between MFC/NFC and coating pigment/latex compared with conventional CMC.

■ CONCLUSIONS

Partial substitution of CMC with MFC/NFC would allow the introduction of new types of rheology modifiers in coating colors, which could bring improved strength properties on the paper surface. Retained fibrous material becomes swollen in water, and the nanofibrillar fraction forms a gel structure containing water within the nanoporous structure. The rheological measurements, oscillatory tests, structure recovery (3ITT), and dynamic dewatering measurements (IMC) indicate distinctly different behavior when polymeric CMC is partially replaced with MFC/NFC. The difference in rheological and dewatering behavior for nanocellulose-based coating is not affected directly by the pigment type, i.e., pigment or pigment blend in the coating formulation. The reason for this is considered to be that nanocellulose, being highly anionic and surrounded by and in bound water, is not easily adsorbed onto pigments and so acts as an independent water-concentrating medium to form a gel. Rheological parameters, viscosity, and elasticity of such coating colors are, as a result, characterized by low friction between the water surrounded nanocellulose (i.e., easier sliding between fibrils) and pigments, with a high degree of shear thinning and particle mobility.

Nanocellulose-based coatings are predicted to show a tendency toward sagging but have good leveling characteristics because they have flow mobility as well as improved freedom for diffusion compared to CMC coatings. Thus, there is a potential for balancing these properties when blending CMC, or other flocculating thickeners, with NFC.

Both gravimetric and dynamic dewatering results show a decrease in the water retention properties for coating colors, which have nanocellulose as part of the cobinder. Once again, the proposed reason for this might be that nanocellulose neither adsorbs on pigment particles nor induces flocculation within the coating color matrix, which helps phase separation or increased mobility of the coating color. A resultant too rapid dewatering, however, could cause problems because the dewatering rate is one of the most important factors controlling formation of the coating structure. However, the more rapid dewatering could allow immobilization to be rapidly implemented and so sagging decreased if a high enough solids concentration can be applied. MFC/NFC, as part of the cobinder formulation, offers a means to change the rheological and water-holding properties dramatically, and the key to these effects is the gel formation with water rather than the flocculating effect of traditional water retention aids.

■ AUTHOR INFORMATION

Corresponding Author

*E-mail: katarina.dimic.misic@aalto.fi.

Notes

The authors declare no competing financial interest.

■ REFERENCES

(1) Turbak, A. F.; Snyder, F. W.; Sandberg, K. R. Microfibrillated Cellulose—A New Composition of Commercial Significance. . *Nonwovens Symp. Notes* **1984**, 115−123.

(2) Agoda-Tandjawa, G.; Durand, S.; Gaillard, C.; Garnier, C.; Doublier, J.-L. Rheological behaviour and microstructure of micro-fibrillated cellulose suspensions/low-methoxyl pectin mixed systems. Effect of calcium ions. *Carbohydr. Polym.* **2012**, *2*, 1045−1057.

(3) Saito, T.; Nishiyama, Y.; Putaux, J.; Vignon, M.; Isogai, A. Homogeneous suspensions of individualized microfibrils from TEMPO-catalyzed oxidation of native cellulose. *Biomacromolecules* **2006**, *6*, 1687−1691.

(4) Ahola, S.; Myllytie, P.; Österberg, M.; Teerinen, T.; Laine, J. Effect of polymer adsorption on cellulose nanofibril water binding capacity and aggregation. *Bioresources* **2008**, *4*, 1315−1328.

(5) Pääkko, M.; Ankerfors, M.; Kosonen, H.; Nykänen, A.; Ahola, S.; Österberg, M.; Ruokolainen, J.; Laine, J.; Larsson, P. T.; Ikkala, O.; Lindström, T. Enzymatic hydrolysis combined with mechanical shearing and high-pressure homogenization for nanoscale cellulose fibrils and strong gels. *Biomacromolecules* **2007**, *6*, 1934−1941.

(6) Siqueira, G.; Bras, J.; Dufresne, A. Luffa cylindrica as a lignocellulosic source of fiber, microfibrillated cellulose and cellulose nanocrystals. *Bioresources* **2010**, *2*, 727−740.

(7) Iwamoto, S.; Abe, K.; Yano, H. The effect of hemicelluloses on wood pulp nanofibrillation and nanofiber network characteristics. *Biomacromolecules* **2008**, *3*, 1022−1026.

(8) Syverud, K.; Stenius, P. Strength and barrier properties of MFC films. *Cellulose* **2009**, *1*, 75−85.

(9) Zimmermann, T.; Bordeanu, N.; Strub, E. Properties of nanofibrillated cellulose from different raw materials and its reinforcement potential. *Carbohydr. Polym.* **2010**, *4*, 1086−1093.

(10) Petersson, L.; Oksman, K. Comparing layered silicates and microcrystalline cellulose as nanoreinforcement. *Compos. Sci. Technol.* **2006**, *13*, 2187−2196.

(11) Pääkkö, M.; Vapaavuori, J.; Silvennoinen, R.; Kosonen, H.; Ankerfors, M.; Lindström, T.; Berglund, L. A.; Ikkala, O. Long and entangled native cellulose I nanofibers allow flexible aerogels and hierarchically porous templates for functionalities. *Soft Matter* **2008**, *12*, 2492−2499.

(12) Saito, T.; Isogai, A. TEMPO-mediated oxidation of native cellulose. *Appita Annu. Conf. Proc.* **2005**, *3*, 337−340.

(13) Lee, S.; Mohan, D. J.; Kang, I.; Doh, G.; Lee, S.; Han, S. O. Nanocellulose reinforced PVA composite films: Effects of acid treatment and filler loading. *Fibers Polym.* **2009**, *1*, 77−82.

(14) Dimic-Misic, K.; Puisto, A.; Gane, P. A.; Nieminen, K.; Alava, M.; Paltakari, J.; Maloney, T. The role of MFC/NFC swelling in the

rheological behaviour and dewatering of high consistency furnishes. *Accepted Cellulose* **2013**.
(15) Karppinen, A.; Vesterinen, A. H.; Saarinen, T.; Pietikäinen, P.; Seppälä, J. Effect of cationic polymethacrylates on the rheology and flocculation of microfibrillated cellulose. *Cellulose* **2011**, *18*, 1381−1390.
(16) Gane, P. A. C.; McGenity, P. M.; Watters, P. Factors influencing the runnability of coating colors at high speed. *Tappi J.* **1992**, *5*, 61−73.
(17) Gane, P. A. C.; Ridgway, C. J.; Schölkopf, J.; Bousfield, D. Heat transfer through calcium carbonate-based coating structures: observation and model for a thermal fusing process. *J. Pulp Paper Sci.* **2007**, *2*, 60−70.
(18) Bluvol, G.; Kässberger, M.; Reichhart, F. Optimizing solids and rheology in blade coating using pigment blends-part. *O PAPEL* **2011**, *11*, 55−59.
(19) Jäder, J.; Järnström, L.; Engström, G. The immobilization cell revisited: Prediction of dewatering kinetics and immobilised layer properties for coating colours. *Nord. Pulp Pap. Res. J.* **2003**, *4*, 382−387.
(20) Willenbacher, N.; Hanciogullari, H.; Rädle, M. New laboratory test to characterize immobilization and dewatering of paper coating colors. *Tappi J.* **1999**, *82*, 167−174.
(21) Nowicki, S.; Davis, H.; Scriven, L. Drying and binder migration in coated papers. *Drying Technol.* **1992**, *10*, 925−946.
(22) Whalen-Shaw, M. *Binder Migr. Pap. Paperboard Coat.* **1993**, *5*, 87−92.
(23) Laudone, G. M.; Matthews, G. P.; Gane, P. A. C. Effect of latex volumetric concentration on void structure, particle packing, and effective particle size distribution in a pigmented paper coating layer. *Ind. Eng. Chem. Res.* **2006**, *6*, 1918−1923.
(24) Iyer, R. R.; Bousfield, D. W. The leveling of coating defects with shear thinning rheology. *Chem. Eng. Sci.* **1996**, *20*, 4611−4617.
(25) Gane, P.; Coggon, L. Coating blade geometry: its effect on coating color dynamics and coated sheet properties. *Tappi J.* **1987**, *12*, 87−96.
(26) Eklund, D.; Salminen, P. Water transport in the blade coating process. *Tappi J.* **1986**, *9*, 116−119.
(27) Husband, J. Adsorption and rheological studies of sodium carboxymethyl cellulose onto kaolin: effect of degree of substitution. *Colloids Surf., A* **1998**, *3*, 349−358.
(28) Kugge, C.; Vanderhoek, N.; Bousfield, D. *J.* Oscillatory shear response of moisture barrier coatings containing clay of different shape factor. *Colloid Interface Sci.* **2011**, *1*, 25−31.
(29) McGenity, P.; Gane, P.; Husband, J.; Engley, M. Effects of Interactions between Coating Color Components and Rheology, Water Retention and Runnability. *TAPPI Conf. Proc.* **1992**, *8*, 133−152.
(30) Li, J.; Tanguy, P.; Carreau, P.; Moan, M. Effect of thickener structure on paper-coating color properties. *Colloid Polym. Sci.* **2001**, *9*, 865−871.
(31) Moan, M.; Aubry, T.; Bossard, F. Nonlinear behavior of very concentrated suspensions of plate-like kaolin particles in shear flow. *J. Rheol.* **2003**, *47*, 1493−1504.
(32) Triantafillopoulos, N. G. *Paper coating viscoelasticity and its significance in blade coating*; Tappi Press: Peachtree Corners, GA, 1996; pp 43−55.
(33) Manninen, M.; Nieminen, K.; Maloney, T. The swelling and pore structure of microfibrillated cellulose. *15th Fundam. Res. Symp.* **2013**, *2*, 765−784.
(34) Dimic-Misic, K.; Puisto, A.; Paltakari, J.; Alava, M.; Maloney, T. The influence of shear on the dewatering of high consistency nanofibrillated cellulose furnishes. *Cellulose* **2013**, *20*, 1853−1864.
(35) Läuger, J.; Wollny, K.; Huck, S. Direct strain oscillation: a new oscillatory method enabling measurements at very small shear stresses and strains. *Rheol. Acta* **2002**, *4*, 356−361.
(36) Deka, A.; Dey, N. Rheological studies of two component high build epoxy and polyurethane based high performance coatings. *J. Coat. Technol. Res.* **2012**, *3*, 305−315.
(37) Moan, M.; Page, A.; Carreau, P. J.; Heuzey, M. Rheological behavior of coating colors: Influence of thickener. *Can. J. Chem. Eng.* **2002**, *6*, 1181−1188.
(38) Yziquel, F.; Moan, M.; Carreau, P.; Tanguy, P. Nonlinear viscoelastic behavior of paper coating colors. *Nord. Pulp Pap. Res. J.* **1999**, *14*, 37−47.
(39) Bossard, F.; Moan, M.; Aubry, T. J. Linear and nonlinear viscoelastic behavior of very concentrated plate-like kaolin suspensions. *Rheology* **2007**, *51*, 1253−1267.
(40) Pajari, H.; Koskela, H. Consolidation of coating colors—Experimental studies. *Adv. Coat. Res. Dev. TAAPI* **2010**, *9*, 347−359.
(41) Wollny, K. New rheological test method to determine the dewatering kinetics of suspensions. *Appl. Rheol.* **2001**, *4*, 197−202.
(42) Ovarlez, G.; Rodts, S.; Chateau, X.; Coussot, P. Phenomenology and physical origin of shear localization and shear banding in complex fluids. *Rheol. Acta* **2009**, *8*, 831−844.
(43) Jader, J.; Järnström, L. Calculation of filter cake thickness under condition of dewatering under shear. *Appl. Rheol.* **2003**, *3*, 125−131.
(44) Herschel, W.; Bulkley, R. Measurement of consistency as applied to rubber-benzene solutions. *Proc. Am. Soc. Testing Mater.* **1926**, *26*, 621−633.
(45) Burgos, G. R.; Alexandrou, A. N.; Entov, V. On the determination of yield surfaces in Herschel−Bulkley fluids. *J. Rheol.* **1999**, *43*, 463−475.
(46) Iotti, M.; Gregersen, Ø. W.; Moe, S.; Lenes, M. Rheological Studies of Microfibrillar Cellulose Water Dispersions. *J. Polym. Environ.* **2011**, *1*, 137−145.
(47) Puisto, A.; Illa, X.; Mohtaschemi, M.; Alava, M. Modeling the viscosity and aggregation of suspensions of highly anisotropic nanoparticles. *Eur. Phys. J. E: Soft Matter Biol. Phys.* **2012**, *1*, 1−7.
(48) Illa, X.; Puisto, A.; Lehtinen, A.; Mohtaschemi, M.; Alava, M. J. Transient shear banding in time-dependent fluids. *Phys. Rev. E* **2013**, *2*, 022307.
(49) Divoux, T.; Grenard, V.; Manneville, S. Rheological hysteresis in soft glassy materials. *Phys. Rev. Lett.* **2013**, *1*, 8409−8418.
(50) Lasseuguette, E.; Roux, D.; Nishiyama, Y. Rheological properties of microfibrillar suspension of TEMPO-oxidized pulp. *Cellulose* **2008**, *3*, 425−433.
(51) Richmond, F.; Co, A.; Bousfield, D. The Coating of Nanofibrillated Cellulose onto Paper using Flooded and Metered Size Press Methods. *2012 Pap. Conf. TAPPI* **2012**, 12PAP18.
(52) Sandås, S.; Salminen, P. J.; Eklund, D. Measuring the water retention of coating colors. *Tappi J.* **1989**, *12*, 207.
(53) Yziquel, F.; Moan, M.; Carreau, P.; Tanguy, P. Nonlinear viscoelastic behavior of paper coating colors, Nordic Pulp and Paper Research Journal. *Nord. Pulp Pap. Res. J.* **1999**, *14*, 37−47.
(54) Derakhshandeh, B.; Kerekes, R.; Hatzikiriakos, S.; Bennington, C. Rheology of pulp fibre suspensions: A critical review. *Chem. Eng. Sci.* **2011**, *15*, 3460−3470.
(55) Horvath, A. E.; Lindström, T. J. The influence of colloidal interactions on fiber network strength. *Colloid Interface Sci.* **2007**, *2*, 511−517.
(56) Lindstrom, T. Cellulose suspentions and polyelectrolytes—some kinetic aspects. *Int. Symp. Wood Pulp. Chem., 8th* **1985**, *1*, 121−122.
(57) Fadat, G.; Engström, G.; Rigdahl, M. The effect of dissolved polymers on the rheological properties of coating colours. *Rheol. Acta* **1988**, *3*, 289−297.
(58) Wallström, A.; Järnström, L. The relation between viscoelastic properties of suspensions based on paper coating minerals and structures of the corresponding coating layers. *Nord. Rheol. Conf.* **2004**, *12*, 215−218.
(59) Lindström, T.; Carlsson, G. The effect of chemical environment on fiber swelling. *Svensk Papperstindning Nordisk Cellulosa* **1982**, *3*, 14−20.
(60) Marrucci, G. J. Dynamics of entanglements: A nonlinear model consistent with the Cox−Merz rule. *Non-Newtonian Fluid Mech.* **1996**, *2*, 279−289.

(61) Husband, J. Interactions between ground calcium carbonate pigments and polymer latices. *Nord. Pulp Pap. Res. J.* **2000**, *5*, 382−386.
(62) Usher, S. P.; De Kretser, R. G.; Scales, P. J. Validation of a new filtration technique for dewaterability characterization. *AIChE J.* **2001**, *7*, 1561−1570.